

An active state of the BL Lac Object Markarian 421 detected by INTEGRAL in April 2013^{*}

E. Pian^{1,2,3}, M. Türlér⁴, M. Fiocchi⁵, A. Bazzano⁵, L. Foschini⁶, F. Tavecchio⁶, V. Bianchin¹, R. Boissay⁴, G. Castignani⁷, C. Ferrigno⁴, C.M. Raiteri⁸, M. Villata⁸, V. Beckmann⁹, F. D'Ammando^{10,11,12}, R. Hudec^{13,14}, G. Malaguti¹, L. Maraschi⁶, T. Pursimo¹⁵, P. Romano¹⁶, S. Soldi¹⁷, A. Stamerra³, A. Treves¹⁸, P. Ubertini⁵, S. Vercellone¹⁶, and R. Walter⁴

- ¹ INAF, Istituto di Astrofisica Spaziale e Fisica Cosmica, via P. Gobetti 101, 40129 Bologna, Italy e-mail: elena.pian@sns.it
- ² Scuola Normale Superiore, Piazza dei Cavalieri 7, 56122 Pisa, Italy
- ³ INFN, Sezione di Pisa, Largo Pontecorvo 3, 56127 Pisa, Italy
- ⁴ ISDC, Data Center for Astrophysics of the University of Geneva, Chemin d'Ecogia 16, 1290, Versoix, Switzerland
- ⁵ Istituto di Astrofisica e Planetologia Spaziali, Via Fosso del Cavaliere 100, 00133 Roma, Italy
- ⁶ INAF-Osservatorio Astronomico di Brera, Via Bianchi 46, 23207 Merate (LC), Italy
- ⁷ SISSA-ISAS, Via Bonomea 265, 34136, Trieste, Italy
- ⁸ INAF-Osservatorio Astronomico di Torino, Strada Osservatorio 20, 10025 Pino Torinese (TO), Italy
- ⁹ Centre François Arago, APC, Université Paris Diderot, CNRS/IN2P3, 10 rue Alice Domon et Léonie Duquet, 75205 Paris Cedex 13, France
- ¹⁰ Dipartimento di Fisica, Università degli Studi di Perugia, Via A. Pascoli, 06123 Perugia, Italy
- ¹¹ INFN, Sezione di Perugia, Via A. Pascoli, 06123 Perugia, Italy
- ¹² INAF, Istituto di Radioastronomia, Via P. Gobetti 101, 40129 Bologna, Italy
- ¹³ Astronomical Institute, Academy of Sciences, Fricova 298, 25165 Ondrejov, Czech Republic
- ¹⁴ Czech Technical University in Prague, Faculty of Electrical Engineering, Czech Republic
- ¹⁵ Nordic Optical Telescope, Apartado 474, 38700 Santa Cruz de La Palma, Spain
- ¹⁶ INAF, Istituto di Astrofisica Spaziale e Fisica Cosmica, via U. La Malfa 153, 90146 Palermo, Italy
- ¹⁷ APC, Université Paris Diderot, CNRS/IN2P3, 10 rue Alice Domon et Léonie Duquet, 75025 Paris Cedex 13, France
- ¹⁸ Università degli Studi dell'Insubria, Via Valleggio 11, 22100 Como, Italy

ABSTRACT

Context. Blazars are active and highly variable extragalactic sources, with compact inner engines powered by supermassive black holes and with relativistic jets pointing at small angles with respect to the observer.

Aims. Multi-wavelength variability offers indirect, but most effective, insight into these powerful engines and on the mechanisms through which energy is propagated from the center down the jet. Therefore, monitoring programs of blazars at all frequencies have now reached a remarkable level of sophistication.

Methods. In this context, we activated INTEGRAL observations of the BL Lac object Markarian 421 in an active state on 16-21 April 2013 (total exposure time of 400 ks), and complemented them with Fermi-LAT data.

Results. We obtained well sampled optical, soft and hard X-ray light curves that show the presence of two flares, the first one reaching a brighter maximum than the second one at X-rays, and time-resolved spectra in the 3.5-60 keV (JEM-X and IBIS/ISGRI) and 0.1-100 GeV (Fermi-LAT) ranges. We constructed spectral energy distributions from the optical to the TeV domain that we compared to homogeneous models of blazar emission. The average flux in the 20-100 keV range is 9.1×10^{-11} erg s⁻¹ cm⁻² (~4.5 mCrab) and the nuclear average apparent magnitude, corrected for Galactic extinction, is $V \simeq 12.2$. In the time-resolved spectra we see a change of spectral slope at an energy that correlates with flux, as expected in refreshed energy injections in a population of electrons that cool thereafter via synchrotron radiation. During the observation, the variability level increases monotonically from the optical to the hard X-rays, and the cross-correlation analysis during the onset of the most prominent flare shows an increasing delay of the lower frequencies emission with respect to the higher frequencies, with a maximum time-lag of about 70 minutes, that is however not very well constrained.

Conclusions. The dataset of Mkn 421 presented here displays strong variability in the hard X-rays and GeV gamma-rays during a period of historically high optical state and extreme activity at TeV energies. The rapid spectral variation of the GeV emission requires fast changes of the electron characteristic energy and/or of the magnetic field, thus implying efficient acceleration mechanisms. The multi-wavelength variability in Mkn 421, in particular at X-rays, can be very complex and its patterns may change from epoch to epoch down to intra-day timescales, depending on the emission state, making accurate monitoring of this source necessary.

Key words. galaxies: active — X-rays: galaxies — galaxies: individual: Mkn 421 — radiation mechanisms: non-thermal — gamma-rays: galaxies

^{*} Based on observations obtained with *INTEGRAL*, an ESA mission with instruments and science data center funded by ESA member states (especially the PI countries: Denmark, France, Germany, Italy,

Switzerland, Spain, Czech Republic and Poland), and with the participation of Russia and the USA.

1. Introduction

Blazars are the most luminous persistent sources in the Universe, reaching bolometric luminosities as large as 10^{49} erg/s, often dominated by the gamma-ray output (Ghisellini et al. 2011). They are highly variable, with doubling timescales ranging from seconds to years. Recent dense and accurate monitorings have shown that, while in general the variation amplitudes are higher at shorter wavelengths (e.g., Pian et al. 2011), the multi-wavelength behavior is often more complex and calls into question the role of multiple radiation components (Aleksic et al. 2012; Bonning et al. 2012; D’Ammando et al. 2013). The blazar spectrum is characterized by a thin synchrotron component that peaks, in a νf_ν representation, in the wavelength range from far-infrared to X-rays, and by an inverse Compton component that extends from X-rays to the TeV range, peaking at MeV-GeV energies. These characteristic frequencies vary in an anti-correlated way with respect to bolometric luminosity (Fossati et al. 1998, see however Padovani, Giommi & Rau 2012), leading to a broad distinction of blazars in Low-Frequency-Peaked and High-Frequency-Peaked objects (Padovani & Giommi 1995). Assuming that the emitting region responsible for the emission at X-ray and gamma-ray energies is homogeneous, the ratio between the peak frequencies of the two components represents the characteristic cooling energy of the relativistic particles in the jet plasma (barring Klein-Nishina suppression).

Markarian 421 ($z = 0.031$) is a known bright BL Lac object (Ulrich 1973; Colla et al. 1975) of the High-Frequency-Peaked type, a strong and variable X-ray source up to the hard X-rays, and belongs to the complete sample of X-ray blazars selected above 15 keV by the Swift/Burst Alert Telescope (BAT) survey (Ajello et al. 2009). The absence of strong optical emission lines indicates that photon sources external to the jet, e.g. an accretion disk or a dust torus, are modest and do not contribute significantly to the electron cooling. As a consequence, the synchrotron component peaks at relatively high frequencies also during quiescence (soft-X-rays) and the synchrotron photons are the main targets for Compton up-scattering by the relativistic particles. This synchrotron self-Compton component peaks at very high energies, making this blazar a strong TeV emitter, although the TeV spectrum is often heavily suppressed by the Klein-Nishina effect (Maraschi et al. 1999; Fossati et al. 2008; Mankuzhiyil et al. 2011). Mkn 421 was the target of many multi-wavelength campaigns involving high energy satellites, Cherenkov telescopes and ground-based optical and radio facilities (Takahashi et al. 1996; Maraschi et al. 1999; Malizia et al. 2000; Fossati et al. 2000a,b; Brinkmann et al. 2001; Albert et al. 2007; Lichti et al. 2008; Fossati et al. 2008; Donnarumma et al. 2009; Acciari et al. 2009; Ushio et al. 2009; Tramacere et al. 2009; Horan et al. 2009; Aleksic et al. 2010; Isobe et al. 2010; Abdo et al. 2011; Acciari et al. 2011; Barres de Almeida 2011; Aleksic et al. 2012; Shukla et al. 2012). The variations at X-ray and TeV frequencies are often very well correlated with no measurable delay (Maraschi et al. 1999), but complex intra-day X-ray variability is present (e.g., Tanihata et al. 2001).

Recently, Mkn 421 has undergone a prolonged state of high activity, with a peak around January 2013, and revived episodes in April 2013. Many instruments detected this high state: Swift, Fermi, NuSTAR, MAXI, ground-based optical and TeV (Balokovic et al. 2013; Cortina, & Holder 2013; Paneque et al. 2013; Negoro et al. 2013; Semkov et al. 2013; Krimm et al. 2013), and radio/mm wavelengths (Hovatta et al. 2013). We activated our program for INTEGRAL follow-up of blazars in outburst, and started observing on 16 April 2013. The results of

this campaign are presented here along with those of the simultaneous Fermi-LAT observations.

2. Observations and results

2.1. INTEGRAL

Mkn 421 was observed as a Target of Opportunity by INTEGRAL (Winkler et al. 2003) in the periods 2013 April 16.13-18.58 UT (Revolution 1283) and 19.20-21.68 UT (Rev. 1284) for 200 ks each time. The effective exposure time for IBIS/ISGRI (Ubertini et al. 2003; Lebrun et al. 2003) was 270.9 ks and for JEM-X (Lund et al. 2003) 345.7 ks. We observed in hexagonal dithering mode, so that the source was always in the JEM-X field of view. The screening, reduction, and analysis of the INTEGRAL data have been performed using the INTEGRAL Offline Scientific Analysis (OSA) V. 10.0, publicly available through the INTEGRAL Science Data Center (ISDC, Courvoisier et al. 2003). The algorithms implemented in the software are described in Goldwurm et al. (2003) for IBIS and Westergaard et al. (2003) for JEM-X. The OMC (Mas-Hesse et al. 2003) data, which have been acquired with a standard V-band Johnson filter, have been extracted with default settings, using a 3×3 pixels binning, which is appropriate for point-like sources. Individual measurements that were flagged as problematic were disregarded. The target is well detected.

From the OMC data were subtracted both the contribution of the host galaxy and that of a companion galaxy located at about 14 arc-sec North-East of the nucleus (see Ulrich 1978; Gorham et al. 2000; Nilsson et al. 2007). For the former we adopted $R = 13.29 \pm 0.02$ from Hubble Space Telescope imaging and a color $V - R = 0.63$ (Urry et al. 2000). This magnitude was obtained by integrating the galaxy radial profile to infinity, which is appropriate, considering that the adopted OMC photometric aperture corresponds to a diameter of 50 arc-sec, which is equivalent to infinity for practical purposes (the host of Mkn421 has a half-light radius of only few arc-sec). For the companion galaxy we used the SDSS photometry reported in the NED¹ database (this source is identified as RXJ1104.4+3812:BEV[98]014), converted to the Johnson V band. Our total estimated flux of this satellite galaxy in the V-band is 1.72 ± 0.02 mJy. Finally, we have applied a Galactic extinction correction using $E_{B-V} = 0.014$ (Schlafly & Finkbeiner 2011) and the curve of Cardelli et al. (1989). The corrected OMC fluxes are reported in Figure 1a. Two fully resolved flares of 10-15% amplitude and a duration of ~ 2 days each are detected, with similar increasing and decreasing times. Our average flux is approximately consistent with the photometry obtained just prior to our monitoring (Semkov et al. 2013), and it is more than a factor of 2 larger than measured in June 2006 by Lichti et al. (2008), when account is given for the fact that those authors adopt a somewhat dimmer host galaxy contribution, and do not correct for the presence of the host galaxy companion.

The source is clearly and significantly ($\sigma \gtrsim 10$) detected with JEM-X in most individual pointings. Its average flux corresponds to 26 mCrab. The light curve is reported in Figure 1b in three different bands.

IBIS/ISGRI detected the source significantly in individual science windows (~ 2000 s) only in some occasions, notably during maximum flux on April 17, when it reached $8\text{-}\sigma$ significance in a single science window. The final mosaic yields an average flux in the 20-100 keV range of 1.10 ± 0.05 counts s^{-1} , corresponding to (4.4 ± 0.2) mCrab. The ISGRI light curves in the

¹ ned.ipac.caltech.edu

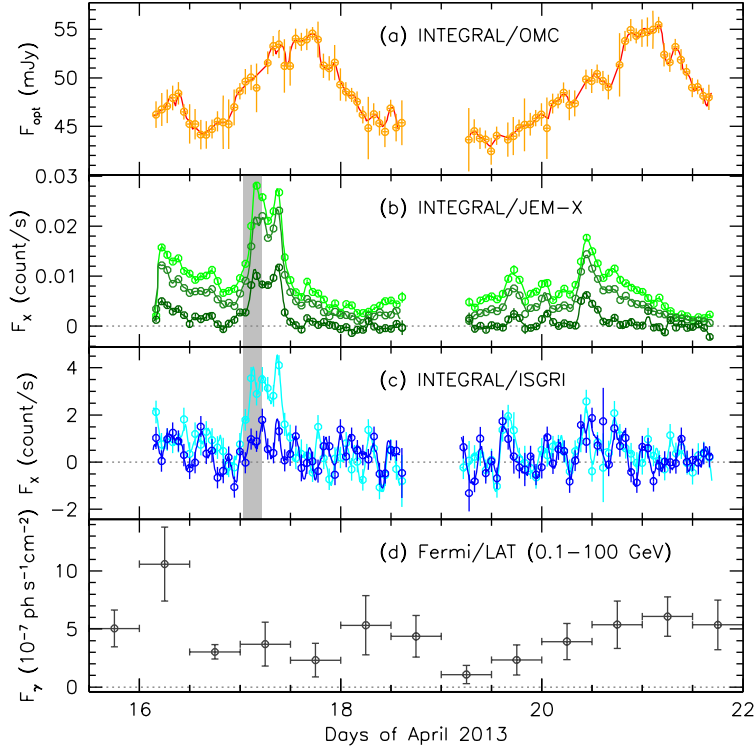


Fig. 1. Light curves of Mkn421 in April 2013: (a) OMC dereddened ($E_{B-V} = 0.014$) photometry, corrected for the host galaxy and for a companion galaxy that is located in the OMC field of view; (b) JEM-X count rates (resulting from the coaddition of the signal measured by the 2 detectors), in the bands 3.04–5.52 keV (light green), 5.52–10.24 keV (green), and 10.24–25.88 keV (dark green); (c) IBIS/ISGRI count rates at 20–40 keV (light blue) and 40–100 keV (dark blue); (d) Fermi-LAT fluxes binned with 12-hr time-resolution. The shaded grey area in panels (b) and (c) represents the interval chosen for the cross-correlation analysis (see Figure 3).

distinct ranges 20–40 keV and 40–100 keV are reported in Figure 1c.

As in the optical band, the X-ray observations display two main outbursts detected, up to ~ 40 keV, with much higher amplitude (a factor of 2–3) and shorter time-scale (~ 1 day). While the flares have similar shape and amplitude in the optical, the first X-ray flare has higher amplitude and approximately symmetrical shape, i.e. equal rising and decaying times, while the second flare rises faster than it decays. The 40–100 keV light curve is affected by large statistical errors, so that assessing variability is difficult.

The overall JEM-X and ISGRI spectra were extracted, combined and, after convolution with the most recent matrices available in OSA V. 10.0, fitted in the energy range 5–60 keV with a single power-law (reduced $\chi^2 = 1.29$) with a photon index $\Gamma = 2.77 \pm 0.03$. A fixed cross-calibration constant between JEM-X and ISGRI of about 1 (Jourdain et al. 2008) was assumed. Photoelectric absorption caused by the neutral hydrogen

along this line of sight ($N_{HI} = 1.43 \times 10^{20} \text{ cm}^{-2}$, Elvis et al. 1989) is negligible at these frequencies, and therefore not corrected for.

In order to study spectral variability in different states of the source, we defined a series of time intervals for which we extracted JEM-X 1 & 2 spectra and ISGRI spectra. We chose to investigate separately the rising and the decaying phases of the two main flares, i.e. the periods April 16.93–17.1 and April 17.42–17.65 for the first flare, and the periods April 20.21–20.48 and April 20.48–20.78 for the second flare. In addition, we selected the time period April 16.13–16.52 to be simultaneous with the highest GeV emission, the extended period of high flux during the first flare from April 17.1 to 17.42 and, finally, an overall quiescent state to increase the signal-to-noise ratio during the period April 17.77 to 19.58 and April 21.04 to 21.7. We then fitted the JEM-X and ISGRI spectra (3.5–60 keV) together with both a single power-law and a broken power-law model. We consider the latter as a purely phenomenological model to test the presence of significant curvature in the spectrum. The fitting was done assuming a fixed inter-calibration constant of unity. The results are

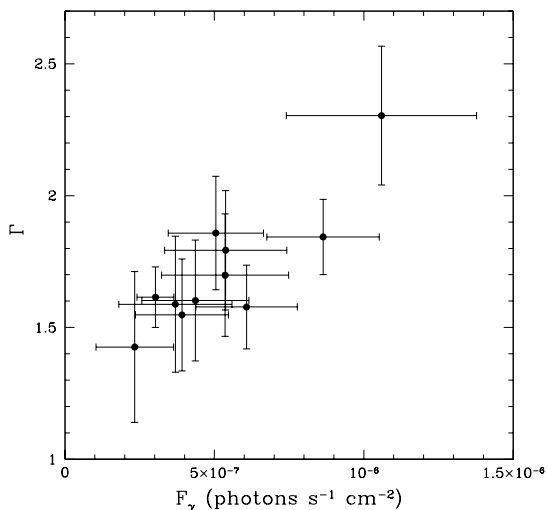


Fig. 2. Fermi-LAT flux (0.1-100 GeV) vs photon index Γ during the campaign. Only measurements for which $TS > 25$ were retained. Note the clear correlation (the linear correlation coefficient is 0.87), indicating that the spectrum hardens when the flux decreases.

reported in Table 1. For all time-resolved JEM-X/ISGRI spectra the broken power-law yields a better fit. This indicates a non-thermal origin of the 3.5-60 keV spectrum, likely due to synchrotron radiation, with a break energy varying between 5 and 10 keV.

2.2. Fermi-LAT

Data of Mkn 421 covering the period 15-22 April 2013 were downloaded from the LAT online public archive² and analyzed with standard methods, as described in <http://fermi.gsfc.nasa.gov/ssc/data/analysis/scitools/>. The adopted software is LAT Science Tools v. 9.27.1, with the Instrument Response Function P7SOURCE_V6 and corresponding files for the Galactic diffuse and isotropic background. The extraction region has a radius of interest of 10 deg and is centered on the radio position of Mkn 421. The sources of the 2FGL catalog present within this radius and Mkn 421 itself were modeled with single power-laws. In order to verify the robustness of the source detection we used the Test Statistics (TS) method (Mattox et al. 1996), taking a threshold of $TS = 9$ (equivalent to about 3σ). The light curve is reported in Figure 1d.

We extracted spectra over time intervals of 12 hours and fitted them to single power-laws ($f(E) \propto E^{-\Gamma}$) in the range 0.1-100 GeV. We see a clear trend of spectral hardening for flux dimming (Figure 2), which is similar to previous behavior seen in Mkn 421 in the period August 2008 - March 2010, and in another blazar of the HBL class, PKS 2155-304 (Foschini et al. 2010). Note that for that same period, Abdo et al. (2011) do not report this correlation for Mkn 421, likely because it cannot be evidenced with integration times of 1 week. For caution, we have verified that by averaging the LAT signal over intervals of 1 day,

the photon indices show the same correlation with flux, although they vary over a narrower range, as expected.

3. Variability and timing analysis

Following Lichti et al. (2008), we evaluated the variability of our multi-wavelength light curves using a fractional rms variability amplitude as defined in Fossati et al. (2000a). As in Lichti et al. (2008), we find increasing variability at increasing energies, although this trend is reverted at the LAT energies, where the fractional variability is less than that computed for IBIS (see Table 2). This is partly due to the relatively large errors of the LAT measurements, but it also matches the fact that the GeV photons are produced by inverse Compton scattering off the electrons that are responsible for the less variable optical spectrum. With respect to Lichti et al. (2008), our variability indices are all larger, indicating larger variability amplitudes in general and a higher level of inter-day and intra-day activity.

We also attempted to cross-correlate the JEMX and ISGRI light curves in search of time lags. We extracted the light curves in various energy ranges in time bins of 300 s for JEM-X and 600 s for IBIS/ISGRI and smoothed these oversampled light curves in a time window of ~ 6 ks with a modified boxcar smooth (Türler, in prep.). The averaging inside the time bins is done by taking into account both the measurement errors and sampling times. More weight is given to points with lower uncertainties and closer to the centre of the time window, making the smoothing robust for light curves with an irregular sampling and unequal errors. We used the Interpolated Cross-Correlation Function (ICCF, Gaskell & Peterson 1987), which is appropriate for curves with no big data gaps, with the improvements introduced by White & Peterson (1994). The time lag corresponds to the maximum of the correlation curve.

In Figure 3 we show the correlation curves of the JEM-X 3.04-5.52 keV light curve with respect to itself (auto-correlation), and with respect to the other bands during the rising phase of the first flare, i.e. when only data in the time window April 17.03-17.21 UT are considered. A negative time lag corresponds to harder photons leading the softer ones. There is a clear and monotonic trend of curves at higher energies leading the JEM-X softest energy curve by larger time lags, with a maximum lag of 72 minutes, although the formal significance is modest, especially for the time lag of the ISGRI 40-100 keV light curve. The $1\text{-}\sigma$ errors, shown in the figure, are obtained by calculating the lag on 1000 perturbed light curves and following the flux-randomization/random subset-selection method described in Peterson et al. (1998). These perturbed light curves were then smoothed and cross-correlated with the ICCF method. We estimated the $1\text{-}\sigma$ statistical uncertainties by taking the boundaries of the region comprising the central 68% of the distribution of their time lags (i.e. $\pm 34\%$ from the median).

We explored other time windows around the first and second flares and did not find more compelling evidence for time delays. In particular, the flare of April 20 suggests a similar trend for JEM-X, but the ISGRI signal is not sufficiently significant, whereas the peak and early decay of the April 17 flare is found to be quasi-simultaneous in all X-ray bands.

Our time lags are comparable in absolute value to those found for Mkn421 in the INTEGRAL observations of June 2006 (Lichti et al. 2008), and to those reported by Sembay et al. (2002), Brinkmann et al. (2003), Ravasio et al. (2004) for the X-rays only (see also Zhang et al. 2004). They are also in line with the report of a much larger time lag, 10 days, of the optical versus X-ray photons (Gaur et al. 2012). These lags can set

² <http://fermi.gsfc.nasa.gov/cgi-bin/ssc/LAT/LATDataQuery.cgi>

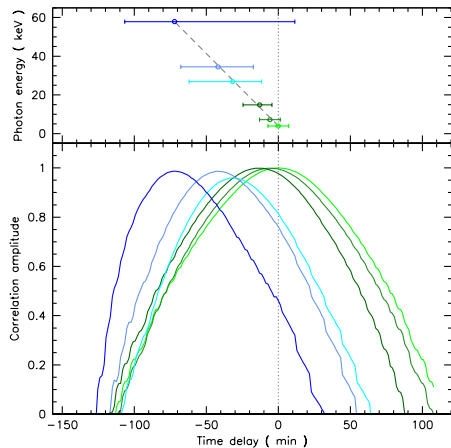


Fig. 3. Cross-correlation function of the INTEGRAL JEM-X (the outputs of the 2 detectors have been coadded) and IBIS light curves during the onset and first peak of the main outburst (April 17.03-17.21 UT). Bottom panel: correlation curves of JEM-X data in the softest range (3.04-5.52 keV) with itself and with the light curves at higher energies, identified by the same colors as in Figure 1. We added here the correlation with the 20–100 keV flux (intermediate shade of blue). Top panel: corresponding correlation time lags as a function of energy (same color-coding as in bottom panel) with $1\text{-}\sigma$ uncertainties based on the distribution of lags obtained by perturbing the original light curves (see Section 3). The energy was evaluated by calculating the average photon energy in the spectral band assuming a photon index of $\Gamma = 2.8$, as obtained by a single power-law fit to the combined JEM-X and ISGRI overall spectra.

Table 2. Fractional rms variability amplitude

Instrument	Band	F_{var}^a
OMC	V-band	0.065
JEMX	3.04-5.52 keV	0.68
JEMX	5.52-10.24 keV	0.85
JEMX	10.24-25.88 keV	1.78
IBIS/ISGRI	20-40 keV	1.42
IBIS/ISGRI	40-100 keV	1.54
Fermi-LAT	0.1-100 GeV	0.35

^a Defined as in Fossati et al. (2000a, Appendix).

important constraints on the cooling times of the relativistic particles responsible for the synchrotron radiation, and in turn on the magnetic field.

The two maxima in the OMC lightcurve might be related to the two main outbursts seen in the X-rays. The overall delay is of ~ 0.5 days, as confirmed by a cross-correlation analysis. We did not try the correlation test on LAT light curve, because of the paucity of flux points.

4. Discussion

We observed and detected Mkn421 with the INTEGRAL instruments IBIS/ISGRI, JEM-X and OMC during a high state

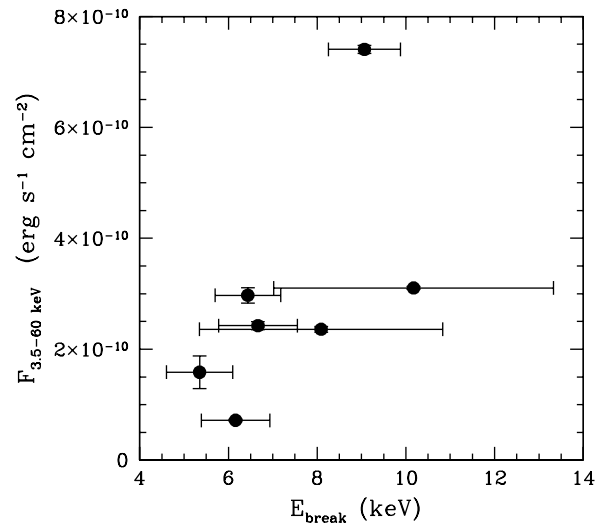


Fig. 4. Flux integrated in the joint JEM-X and IBIS range versus break energy, as derived from the broken power-law spectral fits of time-resolved spectra (Table 1). The linear correlation coefficient is 0.6.

that followed the detection of a powerful TeV energy outburst that was likely subsiding during our observation. The X-ray flux is among the highest previously recorded for this object by INTEGRAL itself (Lichti et al. 2008) and other satellites (Malizia et al. 2000; Donnarumma et al. 2009; Abdo et al. 2011). The optical state is also very bright, with few precedents (Tosti et al. 1998). The LAT state is similar and marginally brighter than detected by Abdo et al. (2011) and a factor of 3 brighter than reported in the 2FGL catalog (Nolan et al. 2012).

Our X-ray spectral fits (Table 1) show that, with respect to the study of Lichti et al. (2008), despite the comparable flux level at the hardest X-rays, we have observed a lower maximum break energy. This parameter never exceeds 10 keV, while the X-ray models of Lichti et al. (2008) can accommodate a break energy higher than ~ 40 keV. The direct correlation of X-ray flux and break energy (Figure 4) is expected from energy injection in the emitting region, that causes both flux enhancement and increase of the break energy. Note that the break energy we derive from the spectral fits represents an estimate of the approximately continuous curvature of the spectra in this region where significant energy losses are taking place. As suggested by both our models and those presented by Lichti et al. (2008), the peak of the νf_ν synchrotron spectrum occurs at lower energies (~ 1 keV in our multi-wavelength models, see Figure 5). We investigated whether there was a difference in the hard X-ray spectrum between the rising and decaying phase of the two outbursts, but could not detect a significant trend within the uncertainties.

We have constructed multi-wavelength spectral energy distributions of Mkn 421 from optical to gamma-rays in three representative states (Figure 5): the first state refers to the initial phase of our INTEGRAL observation (April 16.13-16.52), when LAT

Table 1. Simultaneous JEM-X and ISGRI spectral fits in the 3.5–60 keV range with a single and a broken power-law model^a.

UT	Γ^b	norm_{PL}^c	χ^2	ν^d	Γ_1	Γ_2	E_{break}^e	norm_{BPL}^c	χ^2	ν
2013 Apr 16.13-16.52	2.56 ± 0.03	0.54 ± 0.03	63.89	32	2.14 ± 0.13	2.84 ± 0.08	6.4 ± 0.7	0.29 ± 0.05	31.63	30
2013 Apr 16.93-17.1	2.58 ± 0.05	0.46 ± 0.04	29.46	32	2.43 ± 0.09	3.0 ± 0.3	10 ± 3	0.37 ± 0.05	22.93	30
2013 Apr 17.1-17.42	2.45 ± 0.02	0.86 ± 0.03	174.32	44	2.17 ± 0.04	2.78 ± 0.06	9.1 ± 0.8	0.56 ± 0.04	83.35	42
2013 Apr 17.42-17.65	2.62 ± 0.07	0.40 ± 0.04	47.94	32	1.8 ± 0.5	3.0 ± 0.2	5.4 ± 0.7	0.12 ± 0.07	34.61	30
2013 Apr 20.21-20.48	2.64 ± 0.06	0.44 ± 0.04	28.06	33	2.3 ± 0.2	2.9 ± 0.2	8 ± 3	0.34 ± 0.06	23.31	31
2013 Apr 20.48-20.78	2.63 ± 0.04	0.52 ± 0.04	62.86	33	2.3 ± 0.1	3.0 ± 0.1	6.7 ± 0.9	0.30 ± 0.05	40.77	31
quiescence^f	2.79 ± 0.05	0.23 ± 0.02	74.75	32	2.37 ± 0.15	3.3 ± 0.2	6.2 ± 0.8	0.13 ± 0.03	54.25	30

^a The epochs marked in boldface are those chosen for representation in Figure 5.

^b Photon index: $f(E) \propto E^{-\Gamma}$.

^c At 1 keV, in photons $\text{s}^{-1} \text{cm}^{-2}$.

^d Degrees of freedom.

^e In keV.

^f The spectral signal was integrated over the two intervals 2013 April 17.77 to 19.58 and April 21.04 to 21.7 UT.

measured the brightest flux and softest spectrum; the second state represents the first INTEGRAL flare (April 17.1–17.42), when the 3.5–60 keV flux was at its brightest and LAT measured an intermediate flux and spectrum; the third state describes the dimmest and hardest LAT measurement of April 19.0–19.5, associated with the quiescent INTEGRAL state (indicated with “quiescence” in Table 1), that we obtained by averaging the flux over two intervals where the 3.5–60 keV flux was lowest. The TeV flux had subsided to quiescence by the time our INTEGRAL observation started, thus we report here the latest flux (1.75 ± 0.25 Crab units at $E > 400$ GeV) of the campaign of the VERITAS Cherenkov telescope (Mukherjee 2013), which, recorded on April 16.3 UT, is quasi-simultaneous with the start of our observation.

We modeled this behavior with a single-zone emitting model with a synchrotron component at lower energies, and a self-Compton scattering at the higher energies (e.g. Tavecchio et al. 2011; see however suggestions that this source may be better described by an inhomogeneous model, Krawczynski et al. 2001; Blazejowski et al. 2005; Ghisellini et al. 2005). Accommodating the softest LAT spectrum and the simultaneous TeV flux proved to be difficult (see Figure 5). While the discrepancy between the model and the TeV flux may be justified by the very high amplitude variability at these energies on short time-scales, the softness of the LAT spectrum is unusual and may command substantial changes in our interpretation of this source.

Relevant model parameters include the minimum, break and maximum energy of the electron energy distribution, γ_{min} , γ_b , γ_{max} , respectively; the indices of the distribution below and above the break energy, n_1 and n_2 , the magnetic field B ; the particle density in the emitting region K , the size of the emitting region or blob R , and the Doppler boosting factor δ . The model parameters are in general similar to those determined by Lichti et al. (2008), Donnarumma et al. (2009), and Abdo et al. (2011) in their multi-wavelength fits with a leptonic model. The very soft LAT spectrum of April 16 implies a significantly higher value of the magnetic field and a relatively low break energy.

The correlation between LAT flux and photon index can be explained if the peak energy of the inverse Compton component crosses the LAT energy range: when it is located at energies lower than the LAT range the flux is higher, while when it moves to energies higher than the LAT range it causes the flux to decrease. Notably, this behavior seems to be only weakly correlated with the X-ray variations (Figure 5).

The signal-to-noise ratio of our light curves is sufficiently high to allow us to analyze the frequency-dependent variability.

Table 3. Model parameters of the multi-wavelength energy distributions

Parameter	April 16 (red ^a)	April 17 (orange)	April 19 (black)
γ_{min}	1000	4000	4000
γ_b	31000	4.1×10^5	1.3×10^5
γ_{max}	5×10^5	2×10^6	1×10^6
n_1	2	2.5	2.5
n_2	3.7	4.9	4.9
B (Gauss)	0.6	0.038	0.04
K (cm^{-3})	1800	1.9×10^5	1.1×10^5
R (cm)	1.7×10^{16}	1.3×10^{16}	1.5×10^{16}
δ	10	40	40

^a Colors refer to the coding in Figure 5.

Our fractional variability parameters indicate increasing variability with frequency and are all higher than those of Lichti et al. (2008). This higher level of activity may also cause the chromatic time lags found with the cross-correlation analysis (Figure 3): the time-lags, albeit affected by big uncertainties, increase with frequency reaching a maximum lag of ~ 72 min between the 40–100 keV and the 3–6 keV flux. The complex multi-wavelength variability observed in Mkn 421 during the present outburst and previous ones occurred and studied over the past years indicates that the source behavior may be dominated by different regimes of injection and cooling in different multi-wavelength states, and thus must be monitored intensively during the transition phases to high states, in order to reconstruct the physical conditions that produce all regimes of variability.

Acknowledgements. We thank Celia Sanchez, Marion Cadolle-Bel, Erik Kuulkers and Chris Winkler of the INTEGRAL Science Operation Center for their assistance with the scheduling of the observations, Lucia Pavan for assistance with JEM-X data calibration, and Imma Donnarumma for helpful discussion. This work was partially supported by ASI/INAF contracts I/009/10/0 and I/088/06/0. This research has made use of the NASA/IPAC Extragalactic Database (NED) which is operated by the Jet Propulsion Laboratory, California Institute of Technology, under contract with the National Aeronautics and Space Administration. This paper is dedicated to the memory of our friend and colleague Paul Barr.

References

- Abdo, A.A., Ackermann, M., Ajello, M., et al. 2011, ApJ, 736, 131
Ajello, M., Costamante, L., Sambruna, R.M., et al. 2009, ApJ, 699, 603
Acciari, V.A., Aliu, E., Aune, T., et al. 2009, ApJ, 703, 169
Acciari, V.A., Aliu, E., Arlen, T., et al. 2011, ApJ, 738, 25
Albert, J., Aliu, E., Anderhub, H., et al. 2007, ApJ, 663, 125
Aleksic, J., Anderhub, H., Antonelli, L.A., et al. 2010, A&A, 519, A32

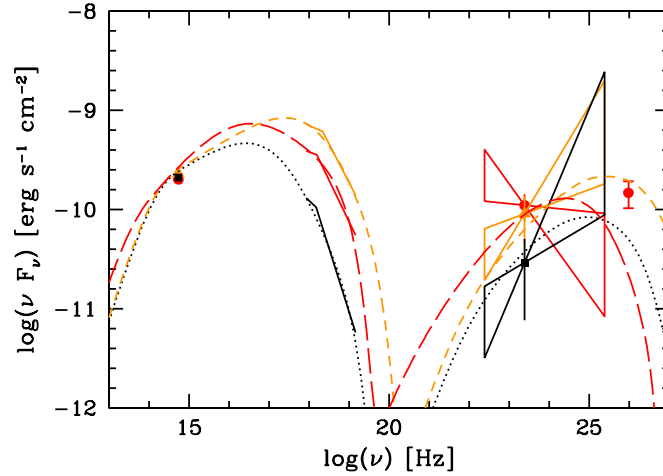


Fig. 5. Spectral energy distributions of Mkn421 at the average UT epochs of 16-16.5 (red circle) and 17-17. (orange triangle) April 2013 and during the quiescent state (black square), that we relate here to the minimum Fermi-LAT flux of April 19.0–19.5, from simultaneous INTEGRAL IBIS/ISGRI, JEM-X and OMC, and Fermi-LAT data. The optical data were corrected for Galactic absorption and for the contamination by galaxies in the field as described in the text. For clarity, the uncertainties of the fitted JEM-X+ISGRI spectra are not reported. The TeV point (red) was taken on April 16.3 and is the last point of the VERITAS observation (Mukherjee 2013). The models (long dash: April 16, short dash: April 17, dot: April 19) include a synchrotron component at the lower energies, produced in a single emitting zone, and a synchrotron self-Compton scattering component at higher energies (see model parameters in Table 3).

- Aleksic, J., Alvarez, E.A., Antonelli, L.A., et al. 2012, *A&A*, 542, A100
Balokovic, M., Furniss, A., Madejski, G., & F. Harrison 2013, ATEL n. 4974
Barres de Almeida, U. 2011, Proceedings of the 32nd International Cosmic Ray Conference (ICRC2011), held 11-18 August, 2011 in Beijing, China. Vol. 8 OG2.3-2.4: Cosmic Ray Origin and Galactic Phenomena, p. 78 (arXiv:1109.5887)
Blazewski, M., Blaylock, G., Bond, I.H., et al. 2005, *ApJ*, 630, 130
Bonning, E., Urry, C.M., Bailyn, C., et al. 2012, *ApJ*, 756, 13
Brinkmann, W., Sembay, S., Griffiths, R.G., et al. 2001, *A&A*, 365, L162
Brinkmann, W., Papadakis, I.E., den Herder, J.W.A., & Haberl, F. 2003, *A&A*, 402, 929
Cardelli, J.A., Clayton, G.C., & Mathis, J.S. 1989, *ApJ*, 345, 245
Colla, G., Fanti, C., Fanti, R., Gioia, I., Lequeux, J., Lucas, R., & Ulrich, M.-H. 1975, *A&AS*, 20, 1
Cortina, J., & Holder, J. 2013, ATEL n. 4976
Courvoisier, T. J.-L., Beckmann, V., Bourban, G., et al. 2003b, *A&A*, 411, L343
Courvoisier, T. J.-L., Walter, R., Beckmann, V., et al. 2003, *A&A*, 411, L53
D'Ammando, F., Antolini, E., Tosti, G., et al. 2013, *MNRAS*, 431, 2481
Dickey, J. M., & Lockman, F. J. 1990, *ARA&A*, 28, 215
Diehl, R., Baby, N., Beckmann, V., et al. 2003, *A&A*, 411, L117
Donnarumma, I., Vittorini, V., Vercellone, S., et al. 2009, *ApJ*, 691, L13
Elvis, M., Lockman, F.J., & Wilkes, B.J. 1989, *AJ*, 97, 777
Foschini, L., Ghisellini, G., Maraschi, L., et al. 2010, 38th COSPAR Scientific Assembly, Event E11, 18-25 July 2012, # E11-0043-10 (Poster, Nr. Sun-093), <http://www.brera.inaf.it/utenti/foschini/COSPAR2010E11/files/foschini.pdf>
Fossati, G., Maraschi, L., Celotti, A., Comastri, A., & Ghisellini, G. 1998, *MNRAS*, 299, 433
Fossati, G., Celotti, A., Chiaberge, M., et al. 2000a, *ApJ*, 541, 153
Fossati, G., Celotti, A., Chiaberge, M., et al. 2000b, *ApJ*, 541, 166
Fossati, G., Buckley, J.H., Bond, I.H., et al. 2008, *ApJ*, 677, 906
Gaskell, C.M., & Peterson, B.M. 1987, *ApJS*, 65, 1
Gaur, H., Gupta, A.C., & Wiita, P.J. 2012, *AJ*, 143, 32
Ghisellini, G., Tavecchio, F., & Chiaberge, M. 2005, *A&A*, 432, 401
Ghisellini, G., Tagliaferri, G., Foschini, L., et al. 2011, *MNRAS*, 411, 901
Goldwurm, A., David, P., Foschini, L., et al. 2003, *A&A*, 411, L223
Gorham, P.W., Van Zee, L., Unwin, S.C., & Jacobs, C. 2000, *AJ*, 119, 1677
Horan, D., Acciari, V.A., Bradbury, S.M., et al. 2009, *ApJ*, 695, 596
Hovatta, T., Balokovic, M., Richards, J.L., Max-Moerbeck, W., & Readhead, A.C.S. 2013, ATEL n. 5107
Isobe, N., Sugimori, K., Kawai, N., et al. 2010, *PASJ*, 62, L55
Jourdain, E., Götz, D., Westergaard, N.J., Natalucci, L., & Roques, J.P. 2008, Proceedings of the 7th INTEGRAL Workshop. 8 - 11 September 2008 Copenhagen, Denmark. Online at <http://pos.sissa.it/cgi-bin/reader/conf.cgi?confid=67>, p.144
Kalberla, P. M. W., Burton, W. B., Hartmann, D., et al. 2005, *A&A*, 440, 775
Krawczynski, H., Sambruna, R., Kohnle, A., et al. 2001, *ApJ*, 558, 187
Krimm, H.A., Barthelmy, S.D., Baumgartner, W., et al. 2013, ATEL n. 4983
Lebrun, F., Leray, J. P., Lavocat, P., et al. 2003, *A&A*, 411, L141
Lichti, G.G., Bottacini, E., Ajello, M., et al. 2008, *A&A*, 486, 721
Lund, N., Budtz-Jørgensen, G., Westergaard, N. J., et al. 2003, *A&A*, 411, L231
Malizia, A., Capalbi, M., Fiore, F., et al. 2000, *MNRAS*, 312, 123
Mankuzhiyil, N., Ansoldi, S., Persic, & Tavecchio, F. 2011, *ApJ*, 733, 14
Maraschi, L., Foscati, G., Tavecchio, F., et al. 1999, *ApJ*, 526, L81
Mas-Hesse, J. M., Giménez, A., Culhane, L., et al. 2003, *A&A*, 411, L261
Mattox, J. R.; Bertsch, D. L.; Chiang, J., et al. 1996, *ApJ*, 461, 396
Mukherjee, R., et al., 2013, "The innermost regions of relativistic jets and their magnetic fields", Granada (Spain), June 10-14, 2013 (http://jets2013.iaa.es/sites/jets2013.iaa.es/files/imagecache/Mukherjee_Granada_jets2013_rev.pdf)
Negoro, H., Suzuki, K., Kawai, N. et al. 2013, ATEL n. 4978
Nilsson, K., Pasanen, M., Takalo, L.O., Lindfors, E., Berdyugin, A., Ciprini, S., & Pforr, J. 2007, *A&A*, 475, 199
Nolan, P.L., Abdo, A.A., Ackermann, M., et al. 2012, *ApJS*, 199, 31
Padovani, P., & Giommi, P. 1995, *ApJ*, 444, 567
Padovani, P., Giommi, P., & Rau, A. 2012, *MNRAS*, 422, L48

- Paneque, D., D'Ammando, F., Orienti, M., & Falcone, A. 2013, ATEL n. 4977
- Peterson, B.M., Wanders, I., Horne, K., Collier, S., Alexander, T., Kaspi, S., & Maoz, D. 1998, PASP, 110, 660
- Pian, E., Ubertini, P., Bazzano, A., et al. 2011, A&A, 526, A125
- Ravasio, M., Tagliaferri, G., Ghisellini, G., & Tavecchio, F. 2004, A&A, 424, 841
- Schlafly, E.F., & Finkbeiner, D.P. 2011, ApJ, 737, 103
- Sembay, S., Edelson, R., Markowitz, A., Griffiths, R.G., & Turner, M.J.L. 2002, ApJ, 574, 634
- Semkov, E., Bachev, R., Strigachev, A., Ibryamov, S., Peneva, S., & Gupta, A.C. 2013, ATEL n. 4982
- Shukla, A., Chitnis, V.R., Vishwanath, P.R., et al. 2012, A&A, 541, A140
- Takahashi, T., Tashiro, M., Madejski, G., et al. 1996, ApJ, 470, L89
- Tanihata, C., Urry, C.M., Takahashi, T., et al. 2001, ApJ, 563, 569
- Tavecchio, F., Ghisellini, G., Bonnoli, G., Foschini, L. 2011, MNRAS, 414, 3566
- Tosti, G., Fiorucci, M., Luciani, M., et al. 1998, A&A, 339, 41
- Tramacere, A., Giommi, P., Perri, M., Verrecchia, F., & Tosti, G. 2009, A&A, 501, 879
- Ubertini, P., Lebrun, F., Di Cocco, G., et al. 2003, A&A, 411, L131
- Ulrich, M.-H. 1973, Ap. Lett. 14, 89
- Ulrich, M.-H. 1978, ApJ, 222, L3
- Urry, C.M., Scarpa, R., O'Dowd, M., Falomo, R., Pesce, J.E., & Treves, A. 2000, ApJ, 532, 816
- Ushio, M., Tanaka, T., Madejski, G., et al. 2009, ApJ, 699, 1964
- Westergaard, N. J., Kretschmar, P., Oxborrow, C. A., et al. 2003, A&A, 411, L257
- White, R.J., & Peterson, B.M. 1994, PASP, 106, 879
- Winkler, C., Courvoisier, T. J.-L., Di Cocco, G., et al. 2003, A&A, 411, L1
- Zhang, Y.-H., Cagnoni, I., Treves, A., Celotti, A., & Maraschi, L. 2004, ApJ, 605, 98